Journal of Colloid and Interface Science 449 (2015) 443–451

Contents lists available at ScienceDirect

Journal of Colloid and Interface Science

www.elsevier.com/locate/jcis

Statistically-based DLVO approach to the dynamic interaction of colloidal microparticles with topographically and chemically heterogeneous collectors

Marina Bendersky [a], Maria M. Santore [b], Jeffrey M. Davis [a,*]

[a] Department of Chemical Engineering, University of Massachusetts Amherst, Amherst, MA 01003, United States
[b] Department of Polymer Science and Engineering, University of Massachusetts Amherst, Amherst, MA 01003, United States

GRAPHICAL ABSTRACT

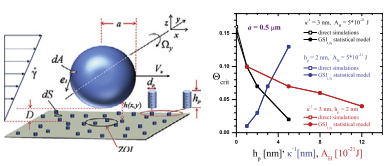

ARTICLE INFO

Article history:
Received 14 November 2014
Accepted 11 February 2015
Available online 21 February 2015

Keywords:
Surface roughness
Particle deposition
Nanoscale heterogeneity
Adhesion thresholds
DLVO interactions

ABSTRACT

Electrostatic surface heterogeneity on the order of a few nanometers is common in colloidal and bacterial systems, dominating adhesion and aggregation and inducing deviations from classical DLVO theory based on a uniform distribution of surface charge. Topographical heterogeneity and roughness also strongly influence adhesion. In this work, a model is introduced to quantify the spatial fluctuations in the interaction of microparticles in a flowing suspension with a wall aligned parallel to the flow. The wall contains nanoscale chemical and topographical heterogeneities ("patches") that are randomly distributed and produce localized attraction and repulsion. These attractive and repulsive regions induce fluctuations in the trajectories of the flowing particles that are critical to particle capture by the wall. The statistical distribution of patches is combined with mean-field DLVO calculations between a particle and two homogeneous surfaces: one with the surface potential of the patches and one with the potential of the underlying wall. These surface potentials could be obtained in experiments from zeta potential measurements for the bare wall and for one saturated with patches. This simple model reproduces the mean DLVO interaction force or energy vs. particle–wall separation distance, its variance, and particle adhesion thresholds from direct simulations of particle trajectories over patchy surfaces. The predictions of the model are consistent with experimental findings of significant microparticle deposition onto patchy, net-repulsive surfaces whose apparent zeta potential has the same sign as that of the particles. Deposition is significantly enhanced if the patches protrude even slightly from the surface. The model predictions are also in agreement with the observed variation of the adhesion threshold with the shear rate in published studies of dynamic microparticle adhesion on patchy surfaces.

© 2015 Elsevier Inc. All rights reserved.

1. Introduction

Deposition morphologies and the dynamic adhesion of colloidal particles [1–6], bacteria [7–9], and cells [10,11] on heterogeneous substrates are typically controlled by chemical and topographical surface features. Even if the surfaces are net-neutral, a nonuniform

* Corresponding author. Fax: +1 413 545 1647.
E-mail address: jmdavis@ecs.umass.edu (J.M. Davis).
URL: http://www.ecs.umass.edu/che/faculty/davis.html (J.M. Davis).

http://dx.doi.org/10.1016/j.jcis.2015.02.031
0021-9797/© 2015 Elsevier Inc. All rights reserved.

charge distribution can significantly alter the colloidal interactions [12]. Similarly, surface roughness can have a pronounced effect and is often implicated for the disagreement between predictions made using classical mean-field DLVO theory and measurements made using atomic force microscopy or electrophoretic mobility at small Debye lengths [13]. Patchy surfaces are representative of chemically and/or topographically heterogeneous substrates encountered in a wide range of industrial and biological process technologies, including packed-bed [14] and membrane filtration applications [15,16], cleaning and coating techniques [17,18], and biosensors [19] and bioelectronic devices composed of biomaterials with information storage capabilities [20]. In these applications, the coupling of particle motion to surface irregularities and electrostatic heterogeneity causes the particle–wall interaction energy to fluctuate around its mean value, and deposition is governed by the minimum energy barrier height instead of its mean value [21].

Estimates of particle deposition rates on heterogeneous surfaces based on a linear patchwise model [22,23] are accurate for patches much larger than the depositing colloidal particles. For surface heterogeneities much smaller than the colloidal particles, however, the predictions of the patchwise model do not agree with experimentally determined deposition rates [24], as some deposition is always predicted if any region of the surface is favorable. By contrast, in experiments with colloidal particles flowing over net-unfavorable surfaces with adsorbed polyelectrolyte chains that form patches of $O(10\text{ nm})$ [3,4,25], deposition is observed only if the areal fraction of the surface covered by the patches, Θ, exceeds a nonzero adhesion threshold, Θ_{crit}. This nonzero threshold indicates that, for patches much smaller than the particles, a group of patches, creating a local "hot spot," is required to adhere a particle. If the patches are replaced by $O(10\text{ nm})$ nanoparticles with similar charge, then particle capture is significantly enhanced [26,27]. Furthermore, it was shown in these experiments that the ionic strength can be used to create a transition from multivalent to univalent particle capture. Multiple nanoparticles arranged to form a local hot spot are required to capture a colloidal particle if the Debye length is smaller than the protrusion of a nanoparticle from the net-unfavorable surface, while a single nanoparticle has been shown capable of capturing a colloidal particle for a Debye length smaller than the nanoparticle. This univalent regime of particle capture corresponds to the disappearance of the adhesion threshold.

While particle deposition studies are often based on simulations that model static (no flow) conditions [2] or on results predicted by dynamic models that do not include the effects of colloidal interactions [28], recent computations based on the trajectories of individual particles have accurately reproduced measured deposition rates and adhesion thresholds [25]. These computations were based on a mobility matrix formulation of the hydrodynamics and the direct computation of electrostatic double layer (EDL) and London-van der Waals (vdW) interactions between the particles and surface [29].

Although direct simulations of particle motion yield experimentally-validated phase space diagrams that delineate dynamic adhesion regimes of skipping, rolling, and arrest [29], this approach is computationally expensive. Many different trajectories must be generated to ensure a statistically meaningful sample of the heterogeneity, and each point in the trajectory of an individual particle requires the computation of DLVO interactions with a particular location on a heterogeneous surface [30]. There is thus a need to predict particle interactions with nanoscale, patchy surfaces without the details of many particle trajectories. Progress has been made through a statistically-based model within the framework of the random sequential adsorption (RSA) approach [3,31], with the number of macro-ions that form a locally-attractive adsorption center a key parameter of the model.

In the present work, a statistical approach is introduced as an alternative method to quantify the effect of randomly-located surface heterogeneities on adhesion thresholds and spatial fluctuations in the potential energy of interaction, which replaces the need for lengthy computations of particle trajectories. This approach requires no assumption of the number of patches involved in particle capture, as the presence of locally attractive regions is determined from DLVO calculations for the patchy surface.

A description of the model is presented in Section 2, and trajectories of particles interacting with patchy surfaces are presented in Section 3. In Section 3.2, attachment efficiency curves are constructed from the trajectories of particles flowing over the heterogeneous collector surface. In Section 4, a statistical model [32] is extended to characterize spatial fluctuations in the particle-collector interaction energy, which enables the identification of local hot spots on net-unfavorable, heterogeneous surfaces without explicit surface construction. This statistical model is then used to determine adhesion thresholds in Section 4.2 and applied to particle adhesion on nanopatterned surfaces. Excellent agreement is found with the trajectory-based approach of Section 3.2. Conclusions are presented in Section 5.

2. Particle–surface interactions

2.1. Description of the model

Presented in Fig. 1(a) is a schematic diagram of the model system, which resembles that used in experimental set-ups [4,5,25]. The flowing particles of radius a are negatively charged, and the collector, or wall, is a negatively-charged, planar surface patterned with positively-charged cylindrical asperities of height h_p and diameter d_p placed at randomly selected locations. This study is limited to the case of asperities that are small relative to the region of the wall that dominates the electrostatic interaction with the particle in the vicinity of contact [30], $d_p, h_p \lesssim O(10\text{ nm})$ for particles with $2a = O(1\ \mu\text{m})$, which is consistent with the cationic nanoparticles used in the experiments [26,27] that motivate this study. The electrostatic potentials of the spherical particle and bottom flat surface are $\psi_{sp} = \psi_s = -26$ mV. The potential of the nano-features ("patches" or "pillars") is $\psi_p = 52$ mV. The local particle–surface separation distance is denoted by h, while D is the minimum separation distance between the particle's surface and either the underlying flat surface or the top of the pillars. Due to the linear shear flow with shear rate $\dot{\gamma}$, the particle translates in the x-direction with velocity V_x and rotates around an axis parallel to the collector surface with rotational velocity Ω_y.

2.2. The GSI technique

The particle–surface colloidal interactions are computed with the Grid-Surface Integration (GSI) [29,30,32] technique, a method that is applicable to particles of arbitrary shape, size, and surface properties and to substrates with chemical and topographical heterogeneities. The GSI technique is related to the Surface Element Integration (SEI) technique, in which the total interaction energy between two bodies is determined by integrating the interaction energy per unit area between two infinite parallel plates [33],

$$P(D) = \iint_{\text{particle}} \widetilde{P}_p(h)\,\mathbf{n}\cdot\mathbf{e}_z\,dA, \tag{1}$$

where $P(D)$ is the interaction energy between the particle and wall at minimum separation distance D, $\widetilde{P}_p(h)$ is the interaction energy

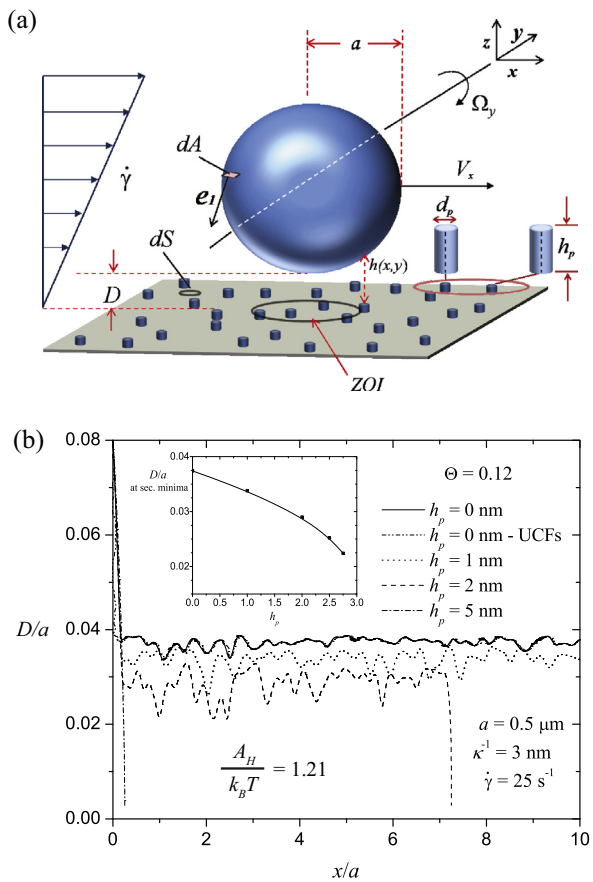

Fig. 1. (a) Schematic diagram of a spherical particle of radius a interacting in shear flow with a heterogeneous surface patterned with nano-pillars of diameter d_p and height h_p. The electrostatic zone of influence (ZOI) is indicated. (b) Trajectories of 1 μm diameter particles interacting in shear flow with heterogeneous surfaces with different h_p for randomly distributed pillars. The parameters are $\Psi_p = 2$, $\Psi_s = \Psi_{sp} = -1$, and $Pe = 6\pi\mu a^3\dot{\gamma}/k_BT = 14.31$, where $\mu \simeq 1 \cdot 10^{-3}$ Pa s is the water viscosity at $T = 298.15$ K. The decrease of D/a at the secondary minima with increasing h_p is shown in the inset. For $h_p = 0$, Brownian motion is computed from Brownian forces (solid line) and from Brownian displacements with UCFs (dash-dot-dot line).

per unit are between two infinite parallel plates separated by a distance h, $\mathbf{e}_z$ is a unit vector normal to the plate, and $\mathbf{n}$ is the outward unit normal vector on the surface element dA of the particle. In the GSI technique, both the particle surface and the heterogeneous (planar) wall are discretized into small areal elements, such that the total interaction (energy or force) between the particle and the heterogeneous surface is obtained by summing the interactions for each pair of discrete areal elements [30],

$$P(D) = \sum_{\text{particle}}\sum_{\text{wall}} \widetilde{P}(h)\,\mathbf{e}_1 \cdot \mathbf{e}_z\, dS, \tag{2}$$

where $P(D)$ is the force or energy for the interaction of the particle and wall at minimum separation distance D, $\widetilde{P}$ is the force or energy per unit area of element dA on the particle with the wall, and dS is the projection of element dA on the wall. As indicated in Fig. 1(a), $\mathbf{e}_1$ is the unit vector that specifies the direction between an element on the wall and an element on the particle, and $\mathbf{e}_z$ is the unit vector normal to the wall. The accuracy of the GSI technique has been confirmed for van der Waals interactions and for electrostatic interactions for conditions of constant surface potentials when the linearized Poisson–Boltzmann equation is valid [30], and this method is well suited to the small asperities considered in the present study. The electrostatic interactions between surfaces with more pronounced topographical features can be accurately computed from the linearized Poisson–Boltzmann equation using a boundary element method [34], with the increased resolution balanced by a significantly increased computational cost and complexity. The application of the GSI technique to electrostatically patchy surfaces is further supported by the accuracy of the Derjaguin approximation for heterogeneous colloidal particles, which has been confirmed experimentally for micrometer-scale silica particles with adsorbed polyelectrolyte dendrimers [35].

The colloidal interactions are calculated for each pair of areal elements from analytical expressions derived for interactions between two infinite parallel plates. The van der Waals interaction energy per unit area between two infinite parallel plates is [36]

$$U_{\text{vdW}}(h) = -\frac{A_H}{12\pi h^2}, \tag{3}$$

where A_H is the non-retarded Hamaker constant for the system and h is the separation distance between the two plates. For conditions of constant surface potential, the energy from the electrostatic double-layer (EDL) interactions between two infinite parallel plates is [37]

$$U_{\text{EDL}}(h) = \frac{\epsilon\kappa}{2}(\psi_{p,1}^2 + \psi_{p,2}^2)\left[1 - \coth(\kappa h) + \left(\frac{2\psi_{p,1}\psi_{p,2}}{\psi_{p,1}^2 + \psi_{p,2}^2}\right)\text{cosech}(\kappa h)\right], \tag{4}$$

where ϵ is the dielectric permittivity of the medium, $\epsilon = 7.08 \times 10^{-10}\ \text{C}^2/\text{Nm}^2$, κ is the inverse Debye screening length and $\psi_{p,1}$, $\psi_{p,2}$ are the dimensional surface potentials of the interacting surfaces. For interactions with surfaces patterned with patches (or pillars) that produce electrostatic and/or topographical heterogeneity, the surface potential, $\psi_{p,2}$ in Eq. (4), and the local separation distance, h in Eqs. (3) and (4), vary with position on the surface. The dimensionless surface potentials are $\Psi_i = ve\psi_i/k_BT$, where $v = 1$ is the charge number, e is the elementary charge, ψ_i is the dimensional surface potential, k_B is the Boltzmann constant, and $T = 298$ K is the temperature. The DLVO forces per unit area (EDL and van der Waals forces) between a particle and a heterogeneous surface are obtained from

$$F(h) = -\frac{\partial U(h)}{\partial h}, \tag{5}$$

and then incorporated into the GSI technique.

2.3. Hydrodynamic interactions

The dynamic profiles of the moving particles are obtained using the method of Duffadar and Davis [30], in which GSI computations of colloidal interactions are incorporated into a mobility tensor formulation of the hydrodynamics problem. The particle's translational velocity $\mathbf{V} \equiv (V_x\ V_y\ V_z)^t$ and rotational velocity $\mathbf{\Omega} \equiv (\Omega_x\ \Omega_y\ \Omega_z)^t$ are determined from the externally applied forces and torques on the sphere due to the shear flow, Brownian motion in the normal and flow directions, and colloidal interactions with the heterogeneous surface. The mobility tensor [38–40] accounts for the fluid's resistance to particle motion, and the underlying hydrodynamic resistance functions are specified elsewhere [30]. The shear-induced force and torque on the particle are determined from asymptotic expressions [38,39] and numerical fits [30]. While the protrusions may be expected to influence the particle velocity when the separation distance becomes comparable to the protrusion scale, this effect has been reported to be $O(d_p/a)$ [41]. Because the role of the shear flow is merely to transport the

particle over the wall, it is assumed that any nano-protrusions on the wall have a negligible influence on the velocity field.

In a simple linear shear flow, the particle translates in the x-direction of flow parallel to the collector surface while rotating about the y-axis. The inertial lift force on the particle is negligible at these low Reynolds numbers [30], so particle motion in the z-direction normal to the collector results only from DLVO interactions and Brownian motion. Brownian effects are incorporated from the stochastic expression [42]

$$F_{\mathrm{Br}} = \frac{k_B T}{a}\,\hat{\eta}, \tag{6}$$

where $\hat{\eta}$ is a random number of the normal standard distribution. Alternatively, Brownian effects could be incorporated through stochastic displacements added to the particle trajectory, with universal correction functions (UCFs) used to account for hydrodynamic effects [43]. As shown in Fig. 1(b) for the case of a 1 μm particle interacting with a flat and electrostatically heterogeneous surface, particle trajectories computed with Brownian forces or Brownian displacements do not exhibit meaningful differences, and the EDL and vdW forces dominate at these small separation distances. The results presented in Sections 3–3.2 are based on Eq. (6). The relative importance of convective transport to Brownian effects is characterized by the Péclet number, $Pe = 6\pi\mu a^3\dot{\gamma}/k_B T$.

3. Results

In this section, the GSI technique is applied to compute trajectories as particles translate under shear flow and interact with a topographically and electrostatically heterogeneous surface. For a given density of pillars or attractive patches, a model heterogeneous surface of 15 μm × 15 μm in size is generated by assigning patches or pillars at randomly selected locations. Once the collector surface is constructed, the centers of flowing particles are initially positioned on the left edge of the collector at randomly sampled locations along the y-axis. The initial separation distance ($D \gtrsim 40$ nm) is sufficiently large that the particles must overcome an energy barrier (associated with the secondary minimum) on the repulsive regions of the surface. The particle trajectories (separation distance vs. distance translated in x) are determined by integrating $d\mathbf{x}/dt = \mathbf{V}$ in time, with $\mathbf{x} \equiv (x, y, z)$ the position of the particle. If the particle–surface separation distance falls below a certain threshold ($D \leqslant \delta = 1$ nm), the particle is considered to be irreversibly adhered to the surface. This value of the limiting distance for adhesion is chosen so that the particle adheres close to the primary minimum (as seen, for example, in Fig. 4(a)). Additional calculations with smaller δ yielded the same results. A simulation is also stopped when a particle translates over the entire collector without adhering.

3.1. Particle trajectories

Trajectories for 1 μm diameter particles flowing over a heterogeneous surface with a fixed surface coverage of $\Theta = 0.12$ and varying pillar heights are shown in Fig. 1(b). For the set of chosen parameters and surfaces with relatively tall pillars, the flowing particles are arrested due to strong attractive interactions, either with the first few pillars the particle encounters ($h_p = 5$ nm) or after translating an horizontal distance of $x \simeq 7a$ ($h_p = 2$ nm). For shorter pillars ($h_p = 0,\ 1$ nm), however, the particles flow over the collector without adhering.

The trajectories exhibit fluctuations independent of Brownian effects that instead arise from variations in the number of patches in the electrostatic zone of influence (ZOI). As $D/a \to 0$, the radius of the zone of influence at leading order is $R_{\mathrm{ZOI}} \sim \sqrt{\kappa^{-1} a}$ [30]. The dynamic behavior is therefore determined by the fluctuating energy landscape as the particle samples the surface, which is induced by the competition between repulsive interactions with the underlying surface and attractive interactions with patches or pillars. Increasing the pillar height strengthens the attractive interactions, decreasing the average particle–surface separation distance D/a and increasing the magnitude of the profiles' fluctuations. The decrease in D/a at the secondary minimum (determined from the mean of U vs. D calculations at many surface locations) with increasing h_p is shown in the inset in Fig. 1(b). These D/a values are in excellent agreement with the arithmetic mean of the separation distance as particles translate with the trajectories shown in Fig. 1(b).

3.2. Attachment efficiency

There are typically two efficiencies defined in colloid filtration theory [44,45]. The collector, or transport, efficiency is dominated by convection and diffusion for Brownian particles and by gravity, fluid drag, and finite-size interception for larger, non-Brownian particles. The usual definition of the (single) collector efficiency is the ratio of the total particle deposition rate on the collector to the rate at which upstream particles approach the projected area of the collector. This collector efficiency therefore provides a quantitative measure of the non-ideality of the phenomena that transport the particles to the collector. By contrast, the attachment efficiency is the ratio of the dimensionless deposition rate of particles on the collector to the rate at which particles are transported to the collector surface, or the fraction of particles that attach to the surface. This attachment efficiency is controlled by the balance between attractive and repulsive forces at length scales smaller than that of the particles. These forces arise from colloidal and chemical interactions. In the absence of an energy barrier in the DLVO interaction energy profile, the attachment efficiency is unity.

The attachment efficiency is most relevant to the present work and is defined as [43]

$$\eta = \frac{N_D}{N_{\mathrm{tot}}}, \tag{7}$$

where N_{D} is the total number of particles deposited on the electrostatically heterogeneous, rough surface and $N_{\mathrm{tot}} = 2000$ is the total number of particles released near the surface. Direct simulations of particle trajectories flowing over surfaces with randomly located asperities are used to determine N_D. Plotting η vs. Θ provides attachment efficiency curves that resemble particle deposition rate curves [5,25,46], but the efficiency curves do not contain any rate information. The adhesion threshold, Θ_{crit}, is defined as the minimum value of Θ for which the attachment efficiency is greater than zero and can be readily found from the attachment efficiency curves from the intercept of the tangent line to the inflection point [4]. In the attachment efficiency computations presented below, for a given value of Θ, the locations of the patches or pillars on the surface and the N_{tot} initial particle positions are identical for different pillar heights and Debye lengths to isolate the influence of h_p or κ^{-1}, respectively, on η.

Attachment efficiency curves for various pillar heights are shown in Fig. 2(a). The adhesion threshold is lower for taller pillars, in qualitative accordance with extensive studies [47–51] that attribute increased particle adhesion rates, or lower overall energies of interaction, to surface roughness. As the pillar height decreases, the attachment efficiency curve broadens. Particle adhesion on surfaces patterned with short pillars depends largely on whether or not the particle encounters a sufficiently large, locally-attractive region as it translates. A few tall pillars, however, are shown to

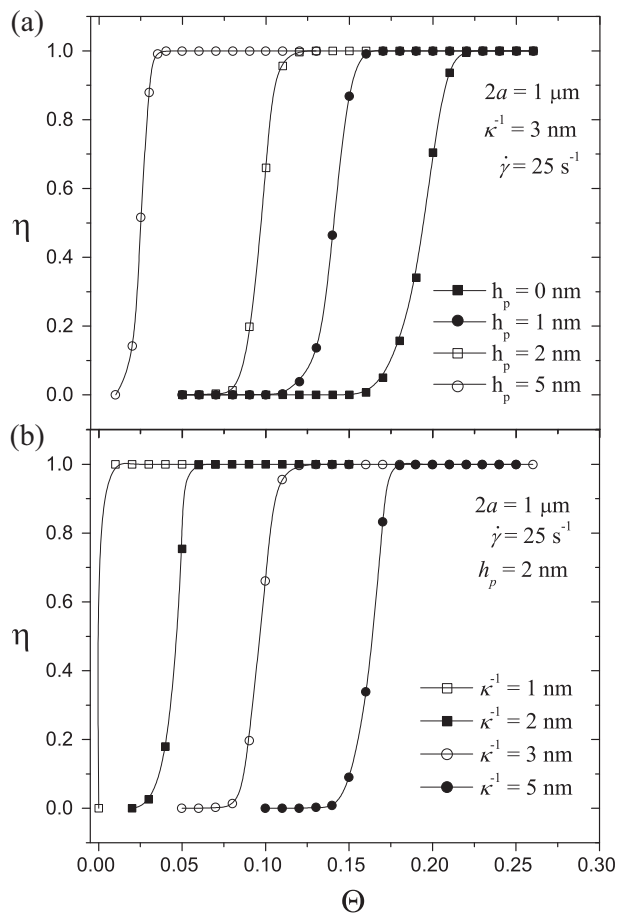

Fig. 2. Attachment efficiency curves for 1 μm particles interacting with heterogeneous surfaces for (a) varying h_p and (b) varying κ^{-1}. The parameters are $\Psi_p = 2$, $\Psi_s = \Psi_{sp} = -1$, $Pe = 14.31$, and $A_H/(k_BT) = 1.21$.

arrest particles effectively (e.g., the particle trajectory for $h_p = 5$ nm in Fig. 1(b)).

In Fig. 2(b), attachment efficiency curves are shown for varying κ^{-1} at constant $h_p = 2$ nm. The curves shift to the right and the adhesion threshold increases for larger values of κ^{-1}. As κ^{-1} is increased, the ZOI is larger, and the particle experiences less localized interactions and more of the average (repulsive) surface charge. For $\kappa^{-1} = 1$ nm, all particles adhere for $\Theta = 0.01$ because the ZOI is small, corresponding to localized EDL interactions, and a few pillars are sufficient to adhere a particle.

4. Analysis via a statistical model

The spatial distribution of the surface heterogeneity determines the distinct adhesive behaviors in colloidal systems that have been observed experimentally [6] and predicted theoretically [29]. The presence of locally-attractive regions within net-repulsive, heterogeneously-charged surfaces explains why those surfaces are often more attractive than initially expected [22,48,50]. Energy fluctuations with varying attractive heterogeneity distributions therefore are key to determining particle adhesion. In this section, the statistical model of Bendersky and Davis [32] is extended to predict the spatial variation of DLVO interactions along heterogeneous surfaces. The standard deviation (at a fixed separation distance) is chosen to characterize the variation in the total DLVO interaction energy for a colloidal particle that samples a substrate with random, nanoscale heterogeneity.

4.1. Fluctuations in interaction energy

The $\mathrm{GSI_{UA}}$ model [32] is derived from the GSI approach [30], in which the interaction energy between a particle and heterogeneous wall is calculated from the sum of pairwise interactions between surface elements on the particle and wall. Selecting one element on the (heterogeneous) wall and performing the sum over all elements on the (uniform) particle in Eq. (2) yields $U = \sum_{i=1}^{N} U_i$, where U_i is the interaction energy between one of the N grid elements on the wall and the entire particle. The expression for U_i depends on the position of the patch on the wall and the distance between the patch and particle. If the grid element corresponds to a patch, $U_i = U_i^{\mathrm{att}}$, which is determined using the surface potential of the (attractive) patch, and analogously for a repulsive element with no patch. The interaction energy is then

$$U = \sum_{i=1}^{N} U_i = \sum_{i=1}^{N} \left[\mathrm{prob}(i = \mathrm{patch}) U_i^{\mathrm{att}} + \mathrm{prob}(i \neq \mathrm{patch}) U_i^{\mathrm{rep}}\right]. \quad (8)$$

This equation is merely a reformulation of the GSI technique and can be applied at any location on the wall (with the probability 1 or 0 for an ordered surface). The key step in the $\mathrm{GSI_{UA}}$ approach is recognizing that the probability that an element on the wall corresponds to a patch is identical to Θ, the fractional areal coverage of the wall by patches, and that each grid element on the wall is indistinguishable with respect to the statistical distribution of patches. This is true only for patches that are randomly distributed on the wall and small compared to the ZOI (so the analysis cannot proceed beyond Eq. (8) for ordered surfaces, such as stripes). For randomly distributed heterogeneity, such as deposited polyelectrolyte patches or nanoparticles,

$$\begin{aligned} U &= \sum_{i=1}^{N} U_i = \sum_{i=1}^{N} \left[\Theta U_i^{\mathrm{att}} + (1-\Theta) U_i^{\mathrm{rep}}\right] \\ &= \Theta \sum_{i=1}^{N} U_i^{\mathrm{att}} + (1-\Theta) \sum_{i=1}^{N} U_i^{\mathrm{rep}} = \Theta U^{\mathrm{att}} + (1-\Theta) U^{\mathrm{rep}}, \end{aligned} \quad (9)$$

where the sum over the N elements on the wall to produce U^{att} and U^{rep} removes the dependence of the particle–wall interaction (U_i) on position, while the dependence on the particle–wall separation distance remains. The mean particle–wall interaction can therefore be determined from a linear combination of two calculations involving uniform collectors: one with the surface potential of a patch (for U^{att}) and one with the potential of the underlying surface (for U^{rep}).

This model can be extended to predict the statistical variation of U over the heterogeneous collector by considering the statistical distribution of patches in the ZOI. The average number of patches (or pillars) in the ZOI is $N_{\mathrm{avg}} = \Theta A_{\mathrm{ZOI}}/A_{\mathrm{patch}}$, where $A_{\mathrm{ZOI}} = \pi R_{\mathrm{ZOI}}^2$ and $A_{\mathrm{patch}} = \pi d_p^2/4$. The number of patches in the ZOI is assumed to be randomly distributed following a Poisson distribution to model particle deposition experiments [4,5] in which the deposition of each new isolated patch is approximately independent of previously deposited patches. Although Θ can be small, the number of patches is sufficiently large ($N_{\mathrm{patches,\,pillars}} > 1000$) that the Poisson distribution can be approximated by a normal distribution $N \sim (\mu = \sigma^2, \sigma)$. This statistical constraint imposes an upper bound on the asperity size for this analysis to be valid,

$$d_{p,\max} \lesssim \sqrt{\kappa^{-1} a}. \quad (10)$$

For larger asperities, the asperity size can significantly influence the particle–wall interactions [e.g., 52]. Within α standard deviations about the mean, the maximum (minimum) number of patches in the ZOI is given by

$$N_{\max/\min} = N_{\text{avg}} \pm \alpha\sqrt{N_{\text{avg}}}, \tag{11}$$

with $\Theta_{\max/\min} = \Theta N_{\max/\min}/N_{\text{avg}}$. The GSI_{UA} can then be used to calculate $U \pm \alpha$ standard deviations by replacing Θ by $\Theta_{\max/\min}$.

For a constant value of h_p, heterogeneous surfaces are generated with an appropriate statistical distribution of heterogeneities, and the standard GSI technique is used to compute U vs. D for $N_{\text{GSI}} = 1000$ distinct heterogeneous surfaces with $\Theta = 0.15$. A large number of surfaces (or surface locations) is required to ensure that the particle samples the statistical distribution of the patches. The arithmetic mean and standard deviation of the interaction energy is then computed for each separation distance D and plotted in Fig. 3. The mean of the N_{GSI} calculations is indistinguishable from the results of the simpler GSI_{UA} model, in agreement with previous results [32]. More significantly, there is excellent agreement between the results for $U \pm \sigma$ determined from the N_{GSI} calculations at different surface locations (for each κD) and the predictions of the statistical GSI_{UA} model with Θ replaced by $\Theta_{\max/\min}$. This simpler statistical approach requires only 2 GSI calculations for homogeneous surfaces yet provides the same information as explicit computations with the N_{GSI} different locations on randomly heterogeneous surfaces. Furthermore, the computation of energy fluctuations for different values of the average surface coverage Θ does not require additional GSI energy-distance simulations. Instead, only the scaling factors $\Theta_{\max}$ and $\Theta_{\min}$ need to be recalculated.

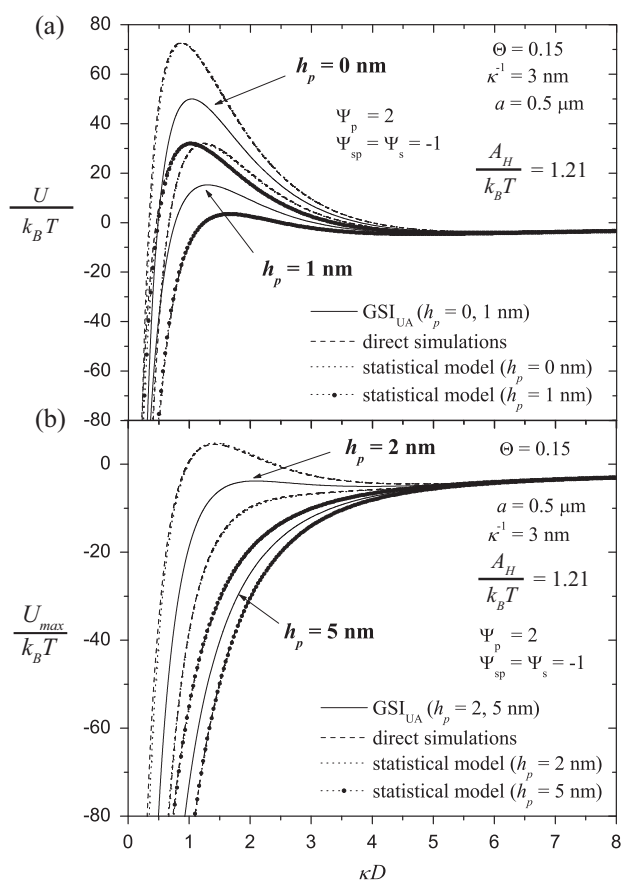

Fig. 3. Mean potential energy of interaction (U) and its standard deviation ($U \pm \sigma$) vs. the normalized separation distance κD. Computed values for U from the GSI_{UA} model and the mean of 1000 direct GSI calculations (for each κD) are indistinguishable (solid curves). Dashed lines indicate $U \pm \sigma$ determined from the 1000 GSI calculations at different locations on the heterogeneous surface. Dotted lines are the predictions of the GSI_{UA} model that requires only 2 GSI calculations for homogeneous surfaces (for each κD).

4.2. Statistical model: Adhesion thresholds

The prediction of adhesion thresholds is of considerable importance to experimental applications involving particle aggregation and deposition. In this section, the statistical model of Section 4 is used to predict adhesion thresholds, and excellent agreement is shown with the results of the particle trajectory simulations in Section 3.2.

To account for the most attractive regions on the surface, corresponding to the largest expected number of patches in the ZOI, Eq. (11) is applied with $\alpha = 3\sqrt{2}$ to determine $N_{\max}$. This value of α was found to give the best agreement with the simulations of particle trajectories. The corresponding maximum surface coverage in a surface region the size of the ZOI is

$$\Theta_{\max} = \Theta\frac{N_{\max}}{N_{\text{avg}}} = \Theta\left(1 + \alpha N_{\text{avg}}^{-1/2}\right). \tag{12}$$

The total interaction energy as a function of the distance D for $\Theta = \Theta_{\max}$ is then computed by applying the GSI_{UA} model. This calculation is simply a linear combination of interactions between the negatively charged sphere and homogeneous positively and negatively charged surfaces with weighting factor $\Theta_{\max}$. A representative energy-distance profile is shown in Fig. 4(a). The energy

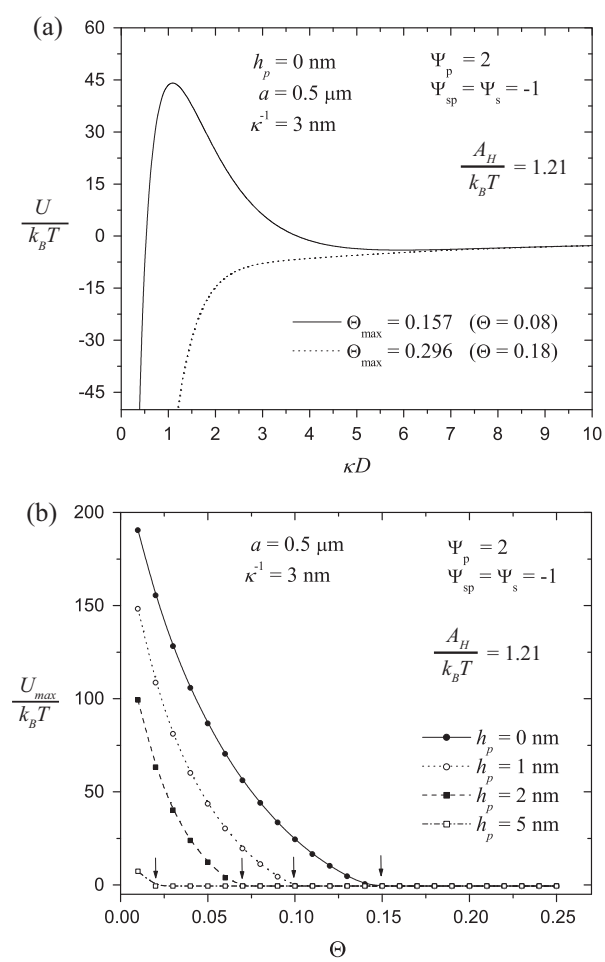

Fig. 4. Energy-averaging statistical model. (a) U vs. κD from the GSI_{UA} model for $\Theta_{\max} = 0.157$ and $\Theta_{\max} = 0.296$, which correspond to $\Theta = 0.08$ and $\Theta = 0.18$ respectively. (b) Dependence of $U_{\max}$ on Θ for various h_p. $U_{\max}$ is the energy barrier of energy-distance profiles, such as that shown in (a), obtained with the GSI_{UA} method and $\Theta_{\max}$. The adhesion threshold Θ_{crit}, determined by the value of the average surface coverage Θ for which $U_{\max}$ vanishes and marked by an arrow, increases as h_p decreases.

Table 1
Agreement between direct simulations (Sim.) of particle trajectories for 1 μm-diameter particles with $\Psi_p = 2$, $\Psi_{sp} = \Psi_p = -1$ and $\dot{\gamma} = 25\ s^{-1}$, and the GSI_{UA} statistical model. The values of the critical surface coverage required for particle adhesion (Θ_{crit}) are shown as a function of the (a) nano-pillar height, with $\kappa^{-1} = 3$ nm and $A_H = 5\times^{-21}$ J, (b) Debye length, with $h_p = 2$ nm and $A_H = 5\times^{-21}$ J, and (c) Hamaker constant, with $\kappa^{-1} = 3$ nm and $h_p = 2$ nm.

(a) h_p [nm]	Sim.	GSI_{UA}	**(b)** κ^{-1} [nm]	Sim.	GSI_{UA}	**(c)** A_H [10^{-21} J]	Sim.	GSI_{UA}
0	0.16	0.15	1	0.01	0.01	1	0.10	0.10
1	0.10	0.10	2	0.03	0.03	5	0.07	0.07
2	0.07	0.07	3	0.07	0.07	8	0.06	0.06
5	0.02	0.02	5	0.13	0.13	12	0.04	0.04

barrier (based on the maximum surface coverage Θ_{max}) is referred to as U_{max}. The maximum surface coverage Θ_{max} is then determined for other average coverages Θ, and U_{max} is determined for each Θ. These calculations simply require the interactions with homogenous surfaces (computed just once) to be scaled by the statistically determined Θ_{max} values, each of which is determined for a specified Θ. The adhesion threshold, $\Theta = \Theta_{crit}$, is the value of Θ at which the energy barrier, U_{max}, vanishes. (For small particles with prominent Brownian effects, deposition may occur with a small energy barrier comparable to the thermal energy of a particle.) In Fig. 4(b), the decrease of U_{max} with increasing Θ is shown for various h_p. It is seen that the addition of pillars only a few nanometers high significantly reduces the energy barrier and the adhesion threshold (indicated by arrows).

The adhesion thresholds determined from this statistical approach are compared in Table 1 to the values obtained by direct simulations in Section 3.2. The agreement is excellent in all of the cases considered. The decrease of the adhesion threshold with increasing h_p, is due to stronger attractive interactions with small numbers of tall pillars, which effectively enhance particle deposition.

The proposed statistical model can easily accommodate variations in the parameters that define the colloidal interactions, such as the Debye length κ^{-1} and the Hamaker constant A_H. As seen from the results presented in Table 1, there is nearly complete agreement between the simulations and the predictions of the statistical model for representative values of κ^{-1} and A_H. The adhesion threshold increases with larger κ^{-1} not only due to stronger electrostatic repulsions at a fixed separation distance but also because the ZOI increases for larger κ^{-1}, such that the particle experiences more of the average (repulsive) interaction from the heterogeneous surface. The adhesion threshold decreases for stronger Van der Waals attractions, represented by larger values of A_H.

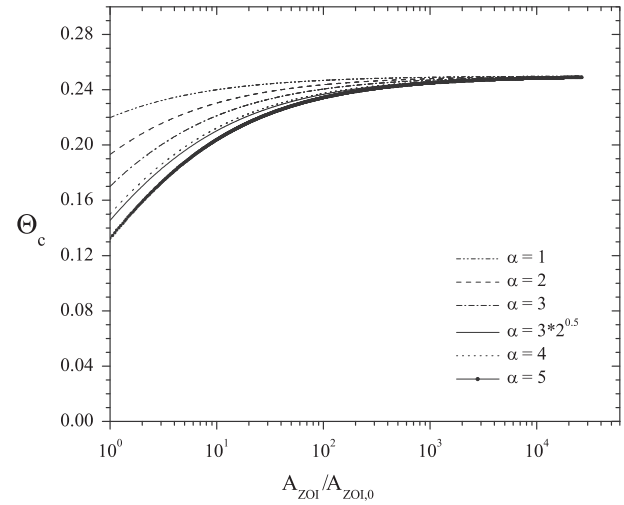

Fig. 6. Adhesion threshold (Θ_c) for varying α as a function of the areas ratio $A_{ZOI}/A_{ZOI,0}$. Other parameters are $a = 500$ nm, $d_p = 10$ nm, $h_p = 0$ nm, $\overline{\Theta} = 0.25$, $\kappa^{-1} = 3$ nm, $A_H = 5\times^{-21}$ J.

Some flow-rate dependence can be imbedded in the parameter α. For larger shear rates, corresponding to a reduced interaction time between a particle and surface feature, adhesion is governed by an effective zone of interaction that is larger than the ZOI and more elongated. The influence of shear rate could be incorporated into α. It is seen from Eqs. (11) and (12) that if the radius of the ZOI is increased by a factor a, $R'_{ZOI} = aR_{ZOI}$, then α is reduced: $\alpha' = \alpha/a$, which corresponds to a smaller value for Θ_{max}. A larger value of Θ is therefore required to attain the same value of Θ_{max} for smaller α, which corresponds to an increase in the adhesion threshold with the shear rate, in qualitative agreement with experiments [46].

If the charge were uniformly distributed, the surface potential of the uniform surface could be expressed in terms of the effective surface loading of a patchy surface, Θ_{avg}, with the same average potential. The effective surface loading when the energy barrier towards adhesion vanishes, $\Theta = \overline{\Theta}$, is defined implicitly by $U_{max}(\Theta = \overline{\Theta}) = 0$, which can be determined from Eq. (9). Plots of $\overline{\Theta}$ vs. κ^{-1} for representative particle sizes and surface potentials are included in Fig. 5. It is seen that the effective surface loading, $\overline{\Theta}$, increases monotonically with the Debye length but does not vary significantly with the particle size. The lower adhesion threshold observed for smaller particles [5] is therefore due primarily to the smaller ZOI, which makes the particles more sensitive to local hot spots on the surface.

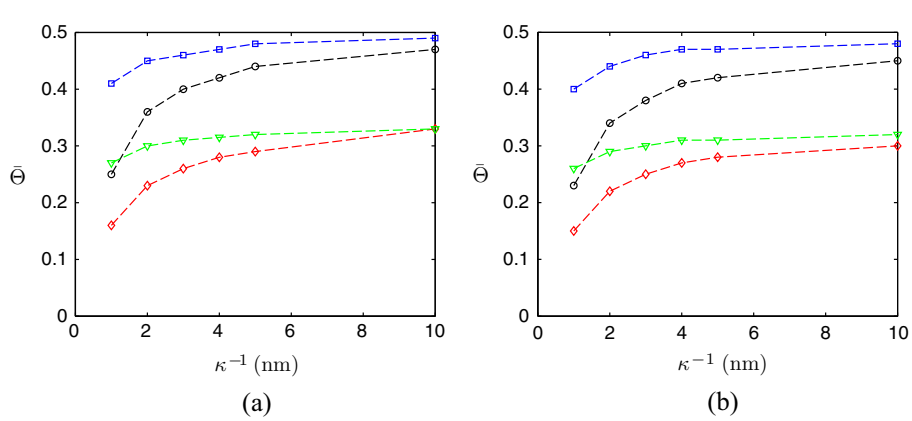

Fig. 5. Effective surface loading $\overline{\Theta}$ when the energy barrier vanishes for a uniform surface plotted against the Debye length κ^{-1} for a particle of diameter (a) $2a = 100$ nm and (b) $2a = 1$ μm for ψ_p/ψ_s [mV] = +25/ − 25 (circles), +50/ − 50 (squares), +50/ − 25 (diamonds), and +100/ − 50 (triangles).

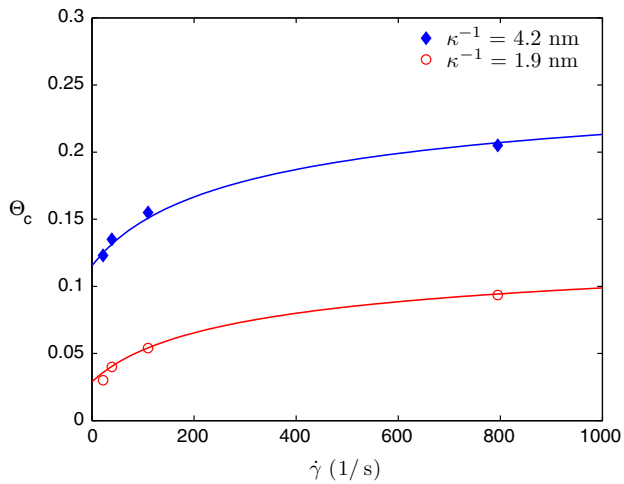

Fig. 7. Adhesion threshold Θ_c plotted against the shear rate $\dot{\gamma}$. The curves are the theoretical predictions from Eq. (14) with $C_h = 1.2 \times 10^{-3}$ μm, and the symbols are the experimental data from Fig. 3 of Kalasin and Stantore [46].

For a patchy surface, the maximum number of patches that can be located within the ZOI is $N_{tot} = A_{ZOI}/A_p$, where A_p is the area of one patch. At the adhesion threshold, $\Theta = \Theta_c$, the surface loading in the ZOI can be approximated as $\overline{\Theta}$ for a uniform surface, which is easy to compute using the GSI_{UA} method. Using Eq. (12) and the definition of N_{avg}, at the adhesion threshold

$$\overline{\Theta} \approx \Theta_{max} = \Theta_c + \alpha\sqrt{\frac{\Theta_c A_p}{A_{ZOI}}}. \tag{13}$$

Solving for Θ_c provides an approximation for the adhesion threshold,

$$\Theta_c^{1/2} = -\frac{\alpha}{2}\sqrt{\frac{A_p}{A_{ZOI}}} + \sqrt{\frac{\alpha^2 A_p}{4A_{ZOI}} + \overline{\Theta}}. \tag{14}$$

For particles being transported over the surface in a shear flow, the effective zone of interaction can be approximated as

$$A_{ZOI} = A_{ZOI,0} + C_h \dot{\gamma} R_{ZOI}, \tag{15}$$

where $A_{ZOI,0}$ is the zone of influence in the absence of fluid flow and C_h is a hydrodynamic constant similar to the parameter introduced by Adamczyk et al. [53].

It is seen from Fig. 6 that Θ_c increases with A_{ZOI}, with $\Theta_c \to \overline{\Theta}$ as $A_{ZOI}/Z_{ZOI,0} \to \infty$. As the effective interaction area becomes large, the particle–wall interactions therefore asymptote to those for uniform surfaces, and the effects of heterogeneity are lost. As α is increased, Θ_c decreases for small A_{ZOI} because adhesion is sensitive to local fluctuations in the patch density.

Eqs. (14) and (15) can be applied for the parameters reported by Kalasin and Santore [46], who studied the influence of shear rate on dynamic microparticle adhesion on electrostatically patchy surfaces. The constant C_h is treated as a fitting parameter. As seen from Fig. 7, the predicted variation of the adhesion threshold with the shear rate is in good agreement with the experimental results. Such agreement is surprising given the simplicity of the model but supports the argument that an increase in the shear rate raises the adhesion threshold not only because of the enhanced hydrodynamic force and torque on a particle [39], which could overcome local adhesive forces, but also because of the increased size of the zone of interaction for dynamic adhesion, which diminishes the influence of small-scale heterogeneity. The influence of shear rate will be treated more rigorously in future work.

5. Conclusion

A statistical model was introduced to calculate DLVO interactions between particles and patchy collectors with nanoscale electrostatic and topographical heterogeneity with a characteristic size much smaller than the electrostatic zone of influence. The patches, which correspond to adsorbed polyelectrolyte chains or nanoparticles in experiments, are randomly distributed on the collector and create localized attractive regions on an otherwise repulsive surface. In this approach, the statistical distribution of patches is combined with DLVO calculations between a particle and two homogeneous surfaces: one with the surface potential of the patches and one with the potential of the underlying collector surface. These surface potentials could be obtained in experiments from zeta potential measurements for the bare collector and for one that is saturated with polyelectrolyte patches. Predictions of the mean interaction energy and its variance as a particle samples the collector are in excellent agreement with the mean and variance of many DLVO calculations for interactions with a heterogeneous collector.

With an appropriately defined zone of influence for the electrostatic-double-layer interactions, the statistical model can predict adhesion thresholds corresponding to the critical surface loading of patches at which particles begin to adhere from flowing solution. These predictions are indistinguishable from the results of computed particle trajectories over heterogeneous surfaces but require only simple DLVO calculations involving homogeneous surfaces that are similar in complexity to a standard, mean-field application of classical DLVO theory. This approach is relevant to studies of particle interaction and deposition onto heterogeneous collectors, particularly those with adsorbed polyelectrolyte patches, and the model successfully predicts the increase in the adhesion threshold with the shear rate of the flowing suspension observed in experiments [46].

The results of the statistical model reveal several reasons patchy surfaces are more attractive toward microparticles than expected. Classical DLVO theory is typically applied with calculations based on a mean (apparent) surface potential, such as the zeta potential measured from electrophoretic mobility or streaming potential experiments, which typically has the same sign as that of the particles when the patch coverage is sparse. A group of patches in close proximity can create a local hot spot capable of capturing a particle, as noted in many studies [3–5,25]. In addition, the mean interaction between the heterogeneous collector and microparticle is less repulsive than predicted by classical DLVO theory because of the random distribution of nanoscale, cationic patches compared to treating the surface charge as uniformly smeared out over the surface. Furthermore, at moderate and large ionic strength, deposition is enhanced significantly if the patches protrude only slightly from the collector. Finally, additional computations were performed for electrostatically-repulsive asperities on an attractive underlying surface. It was found that particle adsorption can sometimes occur on these surfaces, which is consistent with the results of Brownian dynamics simulations of polymer adsorption on patterned surfaces with charge heterogeneity [54]. This behavior will be investigated more extensively in future work.

Acknowledgments

This material is based upon work supported by the National Science Foundation under Grant No. 1264855. JMD also acknowledges support from the Camille Dreyfus Teacher-Scholar Awards Program.

References

[1] Z. Adamczyk, P. Weroński, Adv. Colloid Interface Sci. 83 (1999) 137–226.
[2] Z. Adamczyk, K. Jaszczółt, A. Michna, B. Siwek, L. Szyk-Warszyńska, M. Zembala, Adv. Colloid Interface Sci. 118 (2005) 25–42.
[3] Z. Adamczyk, M. Zembala, A. Michna, J. Colloid Interface Sci. 303 (2006) 353–364.
[4] N. Kozlova, M.M. Santore, Langmuir 22 (2006) 1135–1142.
[5] M.M. Santore, N. Kozlova, Langmuir 23 (2007) 4782–4791.
[6] S. Kalasin, M.M. Santore, Langmuir 26 (2010) 2317–2324.
[7] N. Mohamed, R.R. Rainier, J.M. Ross, Biotechnol. Bioeng. 68 (2000) 628–636.
[8] M.B. Salerno, S. Rothstein, C. Nwachukwu, H. Shelbi, D. Velegol, B.E. Logan, Environ. Sci. Technol. 39 (2005) 6371–6377.
[9] E. Dague, J. Duval, F. Jorand, F. Thomas, F. Gaboriaud, Biophys. J. 90 (2006) 2612–2621.
[10] D.A. Hammer, S.M. Apte, Biophys. J. 63 (1992) 35–57.
[11] M.R. King, R. Sumagin, C.E. Green, S.I. Simon, Math. Biosci. 194 (2005) 71–79.
[12] S.J. Miklavic, D.Y.C. Chan, L.R. White, T.W. Healy, J. Phys. Chem. 98 (1994) 9022–9032.
[13] R.F. Considine, C.J. Drummond, Langmuir 17 (2001) 7777–7783.
[14] K. Yao, M.T. Habibian, C.R. OMelia, Environ. Sci. Technol. 5 (11) (1971) 1105–1112.
[15] Y. Bessiere, D.F. Fletcher, P. Bacchin, J. Membr. Sci. 313 (2008) 52–59.
[16] S. Wang, G. Guillen, E.M.V. Hoek, Environ. Sci. Technol. 39 (2005) 6461–6469.
[17] D. Qi, N. Lu, H. Xu, B. Yang, C. Huang, M. Xu, L. Gao, Z. Wang, L. Chi, Langmuir 25 (2009) 7769–7772.
[18] M.B. Ranade, Aerosol Sci. Technol. 7 (1987) 161–176.
[19] E. Katz, A.F. Bückmann, I. Willner, J. Am. Chem. Soc. 123 (2001) 10752–10753.
[20] I. Willner, M. Lion-Dagan, S. Mam-Tibbon, E. Katz, J. Am. Chem. Soc. 117 (1995) 6581–6592.
[21] J. Czarnecki, Adv. Colloid Interface Sci. 24 (1985) 283–319.
[22] L. Song, P.R. Johnson, M. Elimelech, Environ. Sci. Technol. 28 (1994) 1164–1171.
[23] P.R. Johnson, N. Sun, M. Elimelech, Environ. Sci. Technol. 30 (1996) 3284–3293.
[24] M. Elimelech, J.Y. Chen, Z.A. Kuznar, Langmuir 19 (2003) 6594–6597.
[25] R. Duffadar, S. Kalasin, J.M. Davis, M. Santore, J. Colloid Interface Sci. 337 (2009) 396–407.
[26] J. Zhang, S. Srivastava, R.D. Duffadar, J.M. Davis, V.M. Rotello, M.M. Santore, Langmuir 24 (2008) 6404–6408.
[27] M.M. Santore, J. Zhang, S. Srivastava, V.M. Rotello, Langmuir 25 (2009) 84–96.
[28] T. Rizwan, S. Bhattacharjee, Langmuir 25 (9) (2009) 4907–4918.
[29] R.D. Duffadar, J.M. Davis, J. Colloid Interface Sci. 326 (2008) 18–27.
[30] R.D. Duffadar, J.M. Davis, J. Colloid Interface Sci. 308 (2007) 20–29.
[31] Z. Adamczyk, P. Weroński, E. Musial, J. Colloid Interface Sci. 248 (2002) 67–75.
[32] M. Bendersky, J.M. Davis, J. Colloid Interface Sci. 353 (2011) 87–97.
[33] S. Bhattacharjee, M. Elemelech, M. Borkovec, Croat. Chem. Acta 71 (1998) 883–903.
[34] N. Sun, J.Y. Walz, J. Colloid Interface Sci. 234 (2001) 90–105.
[35] S. Rentsch, R. Pericet-Camara, G. Papastavrou, M. Borkovec, Phys. Chem. Chem. Phys. 8 (2006) 2531–2538.
[36] H.C. Hamaker, Physica 4 (1937) 1058–1072.
[37] R. Hogg, T.W. Healy, D.W. Fuerstenau, Trans. Faraday Soc. 62 (1966) 1638–1651.
[38] A.J. Goldman, R.G. Cox, H. Brenner, Chem. Eng. Sci. 22 (1967) 637–651.
[39] A.J. Goldman, R.G. Cox, H. Brenner, Chem. Eng. Sci. 22 (1967) 653–660.
[40] K. Chang, D.A. Hammer, Langmuir 12 (9) (1996) 2271–2282.
[41] F. Charru, E. Larrieu, J.-B. DuPont, R. Zenit, J. Fluid Mech. 570 (2007) 431–453.
[42] N.A. Mody, M.R. King, Langmuir 23 (2007) 6321–6328.
[43] J.A.L. Kemps, S. Bhattacharjee, Langmuir 25 (12) (2009) 6887–6897.
[44] K.M. Yao, M.T. Habibian, C.R. O'Melia, Enviorn. Sci. Technol. 5 (1971) 1105–1112.
[45] M. Elimelech, C.R. O'Melia, Kinetics of deposition of colloidal particles in porous media, Environ. Sci. Technol. 24 (1990) 1528–1536.
[46] S. Kalasin, M.M. Santore, Langmuir 24 (2008) 4435–4438.
[47] E.P. Ivanova, V.K. Truong, J.Y. Wang, C.C. Berndt, R.T. Jones, I.I. Yusuf, I. Peake, H.W. Schmidt, C. Fluke, D. Barnes, R.J. Crawford, Langmuir 26 (2010) 1973–1982.
[48] M. Hull, J.A. Kitchener, Trans. Faraday Soc. 65 (1969) 3093–3104.
[49] M. Elimelech, C.R. O'Melia, Langmuir 6 (1990) 1153–1163.
[50] L. Suresh, J.Y. Walz, J. Colloid Interface Sci. 183 (1996) 199–213.
[51] J.E. Tobiason, Colloids Surf. 39 (1989) 53–75.
[52] D. Velegol, P.K. Thwar, Langmuir 17 (2001) 7687–7693.
[53] Z. Adamczyk, B. Siwek, L. Szyk, J. Colloid Interface Sci. 174 (1995) 130–141.
[54] N. Hoda, S. Kumar, Langmuir 23 (2007) 1741–1751.